

---

---

# Theranostic Intratumoral Convection-Enhanced Delivery of $^{124}\text{I}$ -Omburtamab in Patients with Diffuse Intrinsic Pontine Glioma: Pharmacokinetics and Lesion Dosimetry

Neeta Pandit-Taskar<sup>1,2</sup>, Pat B. Zanzonico<sup>3</sup>, Milan Grkovski<sup>3</sup>, Maria Donzelli<sup>4</sup>, Scott M. Vietri<sup>1,5</sup>, Christopher Horan<sup>†3</sup>, Brian Serencsits<sup>3</sup>, Kavya Prasad<sup>3</sup>, Serge Lyashchenko<sup>5,6</sup>, Kim Kramer<sup>4,7</sup>, Ira J. Dunkel<sup>4,7</sup>, and Mark M. Souweidane<sup>8,9</sup>

<sup>1</sup>Department of Radiology, Memorial Sloan Kettering Cancer Center, New York, New York; <sup>2</sup>Department of Radiology, Weill Cornell Medical College, New York, New York; <sup>3</sup>Department of Medical Physics, Memorial Sloan Kettering Cancer Center, New York, New York; <sup>4</sup>Department of Pediatrics, Memorial Sloan Kettering Cancer Center, New York, New York; <sup>5</sup>Radiochemistry & Molecular Imaging Probe Core Facility, Memorial Sloan Kettering Cancer Center, New York, New York; <sup>6</sup>Molecular Pharmacology and Chemistry Program, Memorial Sloan Kettering Cancer Center, New York, New York; <sup>7</sup>Department of Pediatrics, Weill Cornell Medical College, New York, New York; <sup>8</sup>Department of Neurosurgery, Memorial Sloan Kettering Cancer Center, New York, New York; and <sup>9</sup>Department of Neurological Surgery, Weill Cornell Medical College, New York, New York

---

J Nucl Med 2024; 65:1364–1370  
DOI: 10.2967/jnumed.123.266365

---

Diffuse intrinsic pontine glioma (DIPG) is a rare childhood malignancy with poor prognosis. There are no effective treatment options other than external beam therapy. We conducted a pilot, first-in-human study using  $^{124}\text{I}$ -omburtamab imaging and theranostics as a therapeutic approach using a localized convection-enhanced delivery (CED) technique for administering radiolabeled antibody. We report the detailed pharmacokinetics and dosimetry results of intratumoral delivery of  $^{124}\text{I}$ -omburtamab. **Methods:** Forty-five DIPG patients who received 9.0–370.7 MBq of  $^{124}\text{I}$ -omburtamab intratumorally via CED underwent serial brain and whole-body PET/CT imaging at 3–5 time points after injection within 4, 24–48, 72–96, 120–144, and 168–240 h from the end of infusion. Serial blood samples were obtained for kinetic analysis. Whole-body, blood, lesion, and normal-tissue activities were measured, kinetic parameters (uptake and clearance half-life times) estimated, and radiation-absorbed doses calculated using the OLINDA software program. **Results:** All patients showed prominent activity within the lesion that was retained over several days and was detectable up to the last time point of imaging, with a mean  $^{124}\text{I}$  residence time in the lesion of 24.9 h and dose equivalent of  $353 \pm 181$  mSv/MBq. Whole-body doses were low, with a dose equivalent of  $0.69 \pm 0.28$  mSv/MBq. Systemic distribution and activities in normal organs and blood were low. Radiation dose to blood was very low, with a mean value of  $0.27 \pm 0.21$  mGy/MBq. Whole-body clearance was monoexponential with a mean biologic half-life of 62.7 h and an effective half-life of 37.9 h. Blood clearance was biexponential, with a mean biologic half-life of 22.2 h for the rapid  $\alpha$  phase and 155 h for the slower  $\beta$  phase. **Conclusion:** Intratumoral CED of  $^{124}\text{I}$ -omburtamab is a novel theranostics approach in DIPG. It allows for delivery of high radiation doses to the DIPG lesions, with high lesion activities and low systemic activities and high tumor-to-normal-tissue ratios and achieving a wide safety margin. Imaging of the actual therapeutic administration of  $^{124}\text{I}$ -omburtamab allows for direct estimation of the therapeutic lesion and normal-tissue-absorbed doses.

**Key Words:**  $^{124}\text{I}$ -omburtamab; DIPG; diffuse intrinsic pontine glioma; convection-enhanced delivery; dosimetry; organ-absorbed doses

**D**iffuse intrinsic pontine glioma (DIPG) is a rare childhood brain malignancy with poor prognosis and a median life expectancy of only 8–10 mo from the time of diagnosis (1,2). Primary treatment includes radiotherapy followed by various clinical trials; however, recurrence is common, and survival rates are poor (1,3,4). Novel treatment strategies are needed to improve outcomes. Our group has used compartmental delivery techniques for administering radiolabeled antibodies in pediatric tumors and has previously reported on the use of  $^{131}\text{I}$ - and  $^{124}\text{I}$ -omburtamab in patients with leptomeningeal disease via intrathecal or intraventricular delivery (5,6). For targeting DIPG, systemic administration or intravenous injections may not be an effective strategy as antibodies generally do not pass through the blood–brain barrier. Similarly, compartmental delivery into the cerebrospinal fluid space is unlikely to deliver adequate labeled antibody to and irradiation of the brain tumor. Direct intratumoral infusion bypasses the blood–brain barrier and is thus more suitable for therapeutic delivery of radiolabeled antibody. A specialized method of intratumoral infusion is convection-enhanced delivery (CED), in which the drug is delivered at a slow rate via a pressure-dependent gradient to enable uniform distribution in the tumor by bulk fluid flow (7). The technique involves infusion through a small-gauge microcannula placed in the tumor under stereotactic guidance (8) and has been used in early-phase clinical studies to deliver chemotherapeutic drugs for treatment of DIPG (9–12).

As a theranostic approach, we administered  $^{124}\text{I}$ -omburtamab intratumorally using CED in patients with DIPG who were previously irradiated without evidence of progression. Omburtamab is a murine IgG1 antibody that binds to antigen B7-H3, a cell-surface glycoprotein expressed in several types of tumors and shown to be overexpressed in DIPG (13,14). Although  $^{124}\text{I}$  is primarily used for PET imaging to assess kinetics and dosimetry and for diagnostic imaging generally, the positron emissions also allow for radiation delivery to tumor cells at therapeutic levels, making it a true theranostic.

---

Received Mar. 13, 2024; revision accepted Jul. 10, 2024.  
For correspondence or reprints, contact Neeta Pandit-Taskar (pandit-n@mskcc.org).  
<sup>†</sup>Deceased.  
Published online Aug. 14, 2024.  
COPYRIGHT © 2024 by the Society of Nuclear Medicine and Molecular Imaging.

Murine studies showed the potential of theranostic administration of  $^{124}\text{I}$ -omburtamab in DIPG using the CED technique (15). On the basis of the preclinical experience, a first-in-human study (NCT-01502917) was initiated at our institution to evaluate the safety and feasibility of CED of  $^{124}\text{I}$ -omburtamab in DIPG. Initial results of this activity-escalation study showed safety and tolerability of activities up to 148 MBq of  $^{124}\text{I}$ -omburtamab (16). This article presents a detailed pharmacokinetic analysis as well as lesion and organ dosimetry in DIPG patients who were treated with escalating activities of  $^{124}\text{I}$ -omburtamab.

## MATERIALS AND METHODS

A phase I theranostic study of CED intratumoral administration of  $^{124}\text{I}$ -omburtamab and PET imaging in patients with progressive DIPG was conducted under an institutionally approved protocol (NCT01502917).  $^{124}\text{I}$ -omburtamab was administered under an Investigational New Drug application (IND# BB-IND 9351) approved by the U.S. Food and Drug Administration. The protocol was approved by our institutional review board and the U.S. Food and Drug Administration. All study patients or their parents or legal guardians provided written informed consent to participate.

### Patients

Patients with confirmed DIPG who had prior radiation (completed at least 4 wk before enrollment) were eligible. Additional eligibility criteria included a performance status of 50 or higher on the Karnofsky or Lansky scale and adequate normal-organ function. Those with progression after radiation therapy, metastatic disease, or symptomatic hydrocephalus were not eligible (16).

### $^{124}\text{I}$ -Omburtamab Radiolabeling

$^{124}\text{I}$ -omburtamab was radiolabeled by the Radiochemistry and Molecular Imaging Probes Core of our institution and in full compliance with the requirements of U.S. Food and Drug Administration.  $^{124}\text{I}$ -omburtamab was prepared as previously described (5,16). The supplemental material provides additional details (supplemental materials are available at <http://jnm.snmjournals.org>).

### Administration

All patients received Cytomel (Pfizer) and supersaturated potassium iodide before infusion of  $^{124}\text{I}$ -omburtamab to prevent free  $^{124}\text{I}$  uptake

in the thyroid. Patients were administered increasing activities of radiolabeled antibody in a standard 3 plus 3 cohort design. For the respective cohorts, the designated administered activity of  $^{124}\text{I}$ -omburtamab ranged from 9.25 to 370 MBq (Table 1) and was delivered in a nearly 1:1 proportionality between volume and activity. The radiolabeled antibody was delivered intratumorally via a slow CED technique, over an hour or longer duration, as required based on calculation using initial infusion rates of 0.05  $\mu\text{L}/\text{min}$  for 10 min, 1.0  $\mu\text{L}/\text{min}$  for 10 min, and 2.0  $\mu\text{L}/\text{min}$  for 10 min for all infusions and with a final rate of 3.5, 5.0, 7.5, or 10.0  $\mu\text{L}/\text{min}$  for the remainder of the volume of injection (Table 1). The administration was done using an automated programmable pump (Harvard Apparatus). The catheter or cannula was removed within an hour after completion of infusion. For all administrations, an extra volume of infusate was dispensed to fill the dead space in the infusion apparatus, including the catheter and canula. After the infusion, the residual activity in the syringe and extension catheter setup were measured in a dose calibrator, and the net administered activity was determined by subtracting the residual activity from the originally dispensed activity.

### $^{124}\text{I}$ -Omburtamab Imaging

Patients underwent PET/CT imaging (GE Discovery STE or GE Discovery 710; GE Healthcare) at multiple time points. Dedicated imaging of the head was performed first, followed by whole-body imaging (vertex to mid thigh) starting 1–4 h after infusion of the radiolabeled antibody and subsequently repeated at 24–48 h, 72–96 h, and at least 1 scan at 96–176 h after infusion. The CT scans performed in conjunction with PET for attenuation correction were low-dose scans (1 scan at a weight-based scaled tube current (mA) for children, 80 mA for adults, and the rest with ultra-low-dose CT at 10 mA). All scans for an individual patient were performed on the same scanner. Emission scans were acquired in 3-dimensional mode at 5 min per bed position for dedicated head imaging and 5–7 min per bed position for the torso.

### PET/CT Image Processing

Images were processed using the manufacturer-provided software. PET images were reconstructed using an ordered-subset expectation maximization algorithm (2 iterations, 16 subsets), time-of-flight information, point-spread-function recovery, and corrections for scatter, random events, and attenuation (CT-based). Scatter correction was performed for processing  $^{124}\text{I}$ -omburtamab scans based on a distribution calculated using a single scatter model, the amplitude of which is

**TABLE 1**  
Patient Demographics and Administered-Activity Cohorts

Cohort	Administered activity level (MBq)*	Number of patients	Age range (y)	Administered activity range (MBq)*	Maximum lesion size (cm)	Volume infused (mL)
1	9.25 (0.25)	3	3–8	8.88–9.99 (0.24–0.27)	3.1–3.3	0.24–0.27
2	18.5 (0.5)	3	5–6; 17	15.9–20.0 (0.43–0.54)	3.1–5.5	0.47–0.63
3	27.75 (0.75)	3	3–7	25.9–27.0 (0.70–0.73)	1.3–4.2	0.69–0.77
4	37 (1.0)	4	3–7; 16, 17	34.8–38.9 (0.94–1.05)	2.3–3.2	0.99–1.05
5	92.5 (2.5)	3	5–6; 17	96.9–98.4 (2.62–2.66)	4.1–4.2	2.56–2.61
6	120.25 (3.25)	3	4–7	117.7–122.1 (3.18–3.3)	3.0–4.1	3.42–3.57
7	148 (4.0)	14	3–11	142.5–158.4 (3.85–4.28)	2.1–5.0	3.84–4.54
8	222 (6)	6	3–8; 12, 16	217.9–243.46 (5.87–6.58)	2.1–4.6	4.18–8.56
9	296 (8)	3	3, 11, 18	281.2–288.6 (7.6–7.8)	2.2–3.6	6.17–8.11
10	370 (10)	2	5, 10	362.6–370.7 (9.83–10.02)	3.6, 3.9	9.71–11.95

\*Activity in mCi given in parentheses.

determined via tail fit. Cascade coincidences were accounted for by including an additional constant parameter when performing the tail fit of the modeled scatter correction (17). The use of a constant during this fit assumes that the cascade coincidence distribution is uniform throughout the projection space (supplemental materials).

### Blood Sampling for Kinetics

Multiple blood samples were obtained, including a baseline sample before infusion of  $^{124}\text{I}$ -omburtamab, and at least 4 additional time points including within 6 h of infusion and within 24–48, 60–96, 120–144, and up to 196 h after infusion; nominal blood sampling time points were the same as the imaging time points. Measured blood aliquots (in mL) were counted in a scintillation well counter (Wallace 1480 Wizard  $\gamma$ -counter; Perkin-Elmer) calibrated for  $^{124}\text{I}$  and the blood counts converted to activity (MBq) and then activity concentration (MBq/L).

Time-dependent blood–activity concentrations were corrected for radioactive decay to the time of infusion. Decay-corrected blood time–activity concentration data were fit to a biexponential function (18). Values of time-integrated activity coefficient concentrations for blood (in h/L),  $\tau$ , were calculated according to the formula  $\tau = \bar{A}/A_0$ , where  $\bar{A}$ , the time-integrated activity concentration, was estimated by integration of the non–decay-corrected time–activity curve and  $A_0$  was the administered activity. Effective and biologic clearance rates and corresponding half-life times were derived from the fitted curves.

The blood mean dose equivalent coefficient (mSv/MBq) was calculated as the product of the time-integrated blood–activity concentration (MBq·s/L) and the mean positron energy per decay ( $3.09 \times 10^{-14}$  Gy kg/Bq·s =  $0.413$  g·rad/ $\mu\text{Ci}\cdot\text{h}$  (19,20)) emitted by  $^{124}\text{I}$  (with adjustment for the units), assuming complete local absorption of the particulate radiation and ignoring the dose contribution of all  $\gamma$ -radiation.

## RESULTS

### Patients and Cohorts

Forty-five patients received intratumoral infusion of  $^{124}\text{I}$ -omburtamab and underwent PET/CT imaging. The age of the patients ranged from 3 to 18 y; the median age was 7 y. Twenty-three patients were boys and 22 were girls. Of the 44 evaluable patients, the dose levels of  $^{124}\text{I}$ -omburtamab were as follows: 9.25 (3 patients), 18.5 (3 patients), 27.25 MBq (3 patients), 37 MBq (4 patients), 92.5 (3 patients), 120.25 MBq (3 patients), 148 MBq (14 patients), 222 MBq (6 patients), 296 MBq (3 patients), and 370 MBq (2 patients) (Table 1). The actual treatment activities, which varied slightly within each dose level, are shown in Table 1. Overall, the administered activity of  $^{124}\text{I}$ -omburtamab ranged from 9.0 to 369 MBq (mean,  $135 \pm 98.5$  MBq). The volumes for the administered doses ranged between 0.24 and 11.95 mL, and the range per cohort is defined in Table 1. The tumor sizes varied from 1.3 and 5.5 cm; cohort-based sizes are also defined in Table 1. The duration of intratumoral administration using slow CED ranged from 1.04 to 21.5 h for all cohorts, with 10 h or longer infusion times for cohort 6 and higher. Initial infusion rates of 0.05  $\mu\text{L}/\text{min}$  for 10 min, 1.0  $\mu\text{L}/\text{min}$  for 10 min, and 2.0  $\mu\text{L}/\text{min}$  for 10 min were used in all patients, with maximal infusion rates of either 3.5  $\mu\text{L}/\text{min}$  ( $n = 5$ ), 5.0  $\mu\text{L}/\text{min}$  ( $n = 14$ ), 7.5  $\mu\text{L}/\text{min}$  ( $n = 13$ ), or 10  $\mu\text{L}/\text{min}$  ( $n = 13$ ) for the remainder of the volume of injection.

### Whole-Body and Blood Kinetics

Whole-body clearance followed a monoexponential pattern; the whole-body biologic clearance had a mean biologic half-life of  $62.7 \pm 17.8$  h (range, 33.3–120 h) (Figs. 1A and 1B). Blood time–activity data followed biexponential functions with an initial increasing uptake phase and later slow clearance phase with a mean biologic

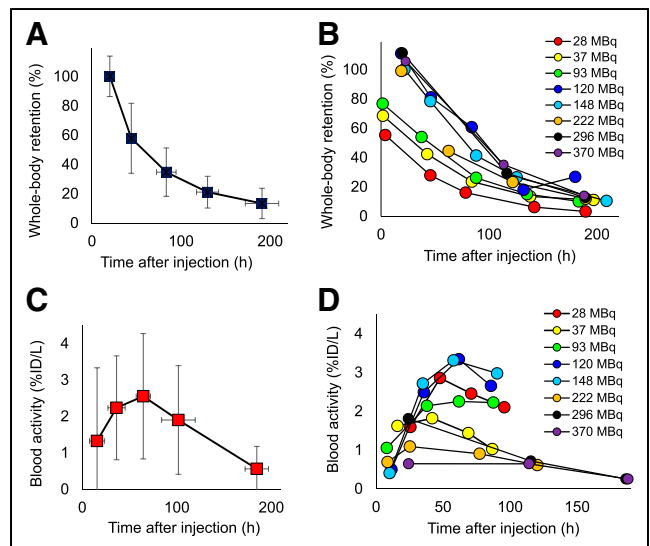


**FIGURE 1.** (A) Whole-body clearance curve for all cohorts. (B) Whole-body clearance curves by cohort. (C) Blood clearance curve of  $^{124}\text{I}$ -omburtamab displayed in aggregate decay-corrected mean values for all patients. (D) Blood clearance curves for patients by cohort. %ID/L = percentage injected dose per liter.

half-life of blood clearance of  $52.2 \pm 14.8$  h (range, 28.8–92.6 h) (Fig. 1A). The blood–activity concentrations were low for all activity cohorts (Figs. 1A and 1B).

### $^{124}\text{I}$ -Omburtamab Normal-Organ Uptake

Initial images showed activity predominantly in the region of the lesion, and activity in the lesion persisted for several days, as visualized on delayed imaging for up to 8 d (Fig. 2). Activity was seen in some patients in the spinal canal in the initial images, clearing with time. Mild tracer activity was visible in the liver and the bladder in all patients 24 h after injection and decreased at later time points. Mild activity was also noted in the thyroid and the stomach in the 24–48 h scans in about half of the patients; the activity decreased at later time points.  $^{124}\text{I}$ -omburtamab biodistribution was characterized by a lack of cardiac or systemic blood-pool activity in the initial images, with mild activity noted in the 24–48 h scans that decreased on later scans. Activity in the urinary bladder was seen in later images, generally 24 h or later. Normal-organ–absorbed doses were low (Table 2). Not surprisingly, normal brain doses were highest among the normal organs, with a mean dose of 4.1 mGy/MBq. Of the distant organs, the urinary bladder received the highest dose, 2.01 mGy/MBq. The liver, thyroid, and stomach wall received doses between 0.92 and 1.15 mGy/MBq. All remaining organs received less than 0.5 mGy/MBq with a total-body absorbed dose and an effective dose of  $0.58 \pm 0.25$  mGy/MBq and  $0.60 \pm 0.28$  mSv/MBq, respectively. The red-marrow dose was low, with a mean dose of  $0.39 \pm 0.17$  mGy/MBq. Cohort-based organ-absorbed doses and normal brain-absorbed doses are presented in Supplemental Table 1.

### Lesion Uptake and Radiation-Absorbed Doses

There was a high concentration of the activity in the lesion with long retention times noted over multiple delayed imaging times (Fig. 2). The mean residence time in the lesions was  $31 \pm 17$  h across all cohorts. The average lesion SUV varied widely, from 364 to 4,756, across the 10 activity cohorts and generally increased

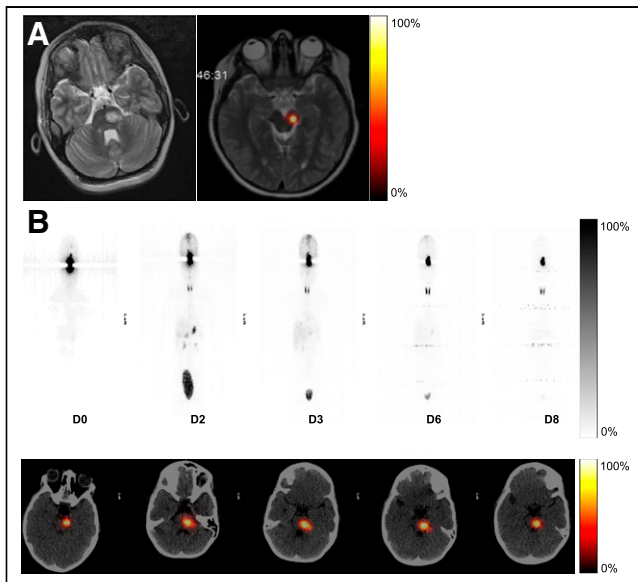


**FIGURE 2.**  $^{124}\text{I}$ -omburtamab lesion and whole-body distribution in 8-y-old female patient. Baseline MRI showing  $1.3 \times 1.2$  cm eccentric mass centered within left lateral pons extending to left cerebral peduncle.  $^{124}\text{I}$ -omburtamab infusion activity was 25.9 MBq. Imaging was performed on day of infusion (D0) and on days 2 (D2), 3 (D3), 6 (D6), and 8 (D8) with whole-body (A) and head imaging (B). High activity is noted at tumor site until last imaging time point (D8). Low activity systemic distribution is noted on D2 as excreted activity in kidneys and bladder, thyroid and stomach, and liver that decreased from D3 to D8.

with increasing administered activity but did not appear to be proportionately related to the administered activity. The biologic clearance in the lesion was either monoexponential with a half-life of  $50 \pm 26$  h or, in most cases, biexponential with an initial slightly faster component and a later slow component with an average half-life of  $36.6 \pm 15$  h for the early component and  $61 \pm 64$  h for the later component; this was more apparent in higher-activity cohorts (level 7 and higher) (Fig. 3A). The mean lesion uptake was  $49 \pm 18$  percent injected dose as measured from the initial imaging and ranging as high as 99%. Uptake in the lesion comprised  $65.6\% \pm 16\%$  of the measured uptake in the whole body at the initial scan.

Lesion-absorbed doses across all cohorts showed a mean absorbed dose of  $353 \pm 181$  mGy/MBq that was calculated using OLINDA's sphere model (Hermes Medical Solutions). The absorbed dose, as expected, increased with higher administered activity. The mean absorbed doses at different cohort levels are shown in Figure 3B. The activity in the body outside of the lesion was very low. The lesion-to-whole-body absorbed-dose ratios were very high, ranging between 172 and 5,051 for all cohorts with a mean ratio of 833 (Fig. 3C).

The  $^{124}\text{I}$ -omburtamab volume of distribution ( $V_d$ ) was equated with the largest volume of interest in and around the infused lesion among the serial  $^{124}\text{I}$ -omburtamab PET scans, as determined by 3-dimensional autosegmentation using a threshold of 40% of the maximum lesion activity concentration (i.e., SUV) with manual adjustments needed in some patients to exclude the extralesional volume. The administered activity within the lesion became more widely dispersed from the injection site with time from the initial imaging to the later imaging times up to day 7 imaging, which was generally most apparent 72–144 h after injection in patients. The volumes of infused activity ( $V_i$ ) increased proportionately with dose escalations among cohorts. The  $V_d$  thus determined was

**TABLE 2**  
Normal-Organ Radiation-Absorbed Dose

Organ or tissue	Absorbed dose (mGy/MBq)			
	Mean	SD	Minimum	Maximum
Adrenal glands	0.38	0.22	0.06	0.98
Brain	4.11	2.09	1.04	9.38
Breasts	0.25	0.14	0.03	0.66
Gallbladder wall	0.43	0.25	0.07	1.01
Lower large intestine wall	0.37	0.23	0.03	0.97
Small intestine	0.38	0.23	0.04	0.97
Stomach wall	1.14	0.93	0.08	3.72
Upper large intestine wall	0.38	0.23	0.04	0.96
Heart wall	0.45	0.24	0.10	1.02
Kidneys	0.37	0.22	0.06	1.11
Liver	0.92	0.77	0.09	3.17
Lungs	0.28	0.14	0.10	0.76
Muscle	0.34	0.18	0.06	0.84
Ovaries	0.39	0.24	0.03	0.98
Pancreas	0.45	0.25	0.06	1.09
Red marrow	0.39	0.17	0.11	0.90
Osteogenic cells	0.60	0.26	0.19	1.36
Skin	0.29	0.14	0.07	0.71
Spleen	0.37	0.24	0.04	1.28
Testes	0.32	0.20	0.02	0.89
Thymus	0.33	0.18	0.06	0.85
Thyroid	1.15	1.12	0.13	7.14
Urinary bladder wall	2.01	2.42	0.08	12.10
Uterus	0.47	0.30	0.04	1.49
Total body	0.58	0.25	0.20	1.22
Effective dose (mSv/MBq)	0.69	0.28	0.26	1.59

linearly correlated with the administered activity and used as a surrogate metric of the  $V_i$  (as the activity concentration in the infusate was the same across all administered-activity cohorts) (Fig. 4). The average and median  $V_d/V_i$  ratios were 3.4 and 3.2, respectively. This linear regression was statistically highly significant ( $P < 0.0005$ ) as determined by ANOVA using the F statistic.

## DISCUSSION

As novel therapeutic approaches are critically needed to treat DIPG, we performed first-in-human theranostic CED infusions with  $^{124}\text{I}$ -omburtamab in DIPG patients. This study is unique in several aspects including the use of  $^{124}\text{I}$ -omburtamab as a novel targeted delivery antibody agent, the use of intratumoral injection, the use of the CED infusion technique, and the use of  $^{124}\text{I}$  alone serving as both a diagnostic and a therapeutic isotope and positrons as therapeutic radiation.

$^{124}\text{I}$ -omburtamab CED infusion was feasible, and the infusion procedure was well tolerated. The highest administered activity and  $V_i$  cohort was 370 MBq, with a  $V_i$  of 10 mL and a maximal

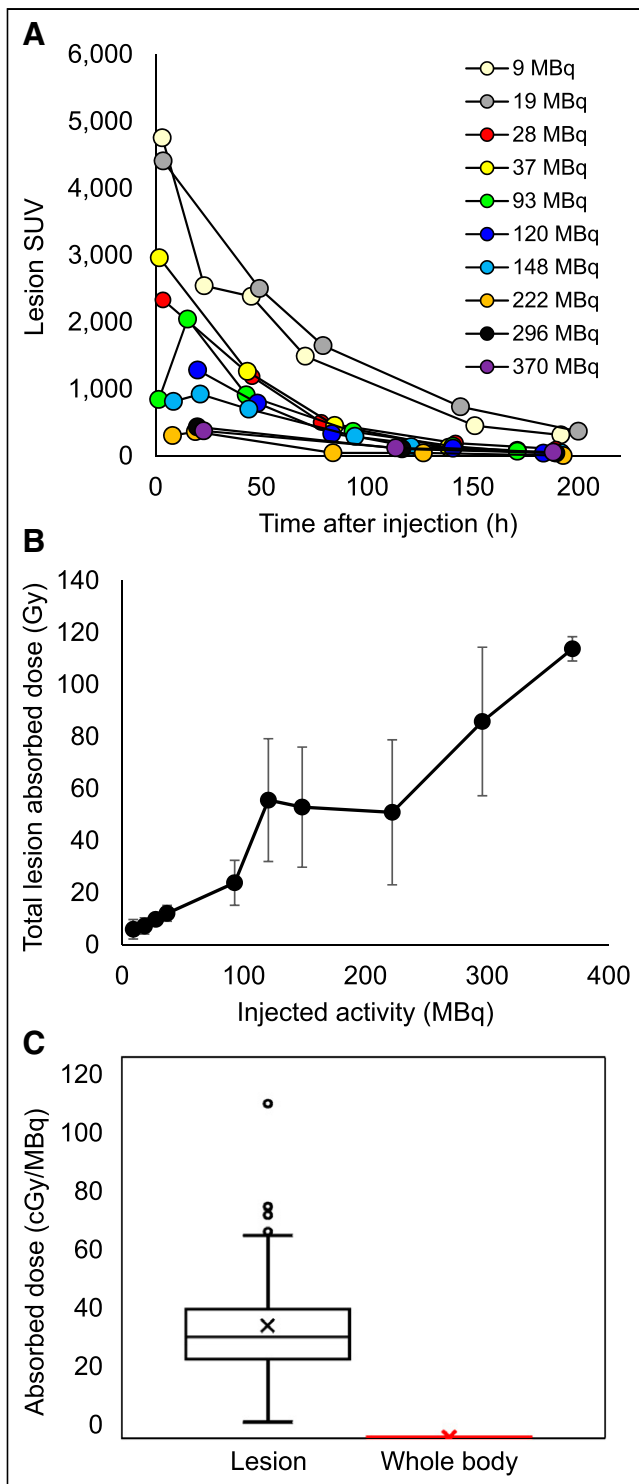


**FIGURE 3.** (A) Lesion uptake and radiation-absorbed dose of  $^{124}\text{I}$ -omburtamab show high concentration within tumor. (B) Radiation-absorbed dose in lesion increases with increased activity over cohorts. (C) Lesion-to-whole-body ratio of radiation-absorbed dose is high, highlighting safe margin and high therapeutic index with local administration.

infusion rate of  $10\ \mu\text{L}/\text{min}$ . Clinical follow-up, survival, and adverse event data have been previously reported for multiple cohorts (16). As previously reported, the treatment was generally well tolerated and the most common treatment-related clinically

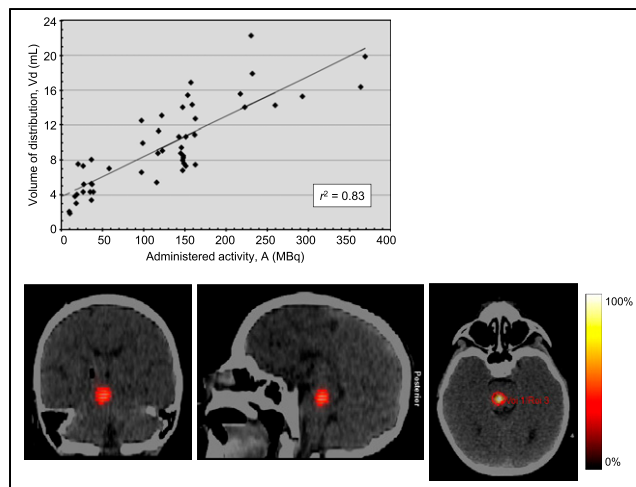


**FIGURE 4.** Distribution volume of administered activity. Linear regression between  $V_d$  (in mL) and administered activity (in MBq) of  $^{124}\text{I}$ -omburtamab, with slope of  $0.046\ \text{mL}/\text{MBq}$ , ordinate intercept of  $3.8\ \text{mL}$ , and correlation coefficient of  $0.83$ . Regression is highly statistically significant ( $P < 0.0005$ ), as determined by ANOVA using F statistic.

significant side effect was transient exacerbation of neurologic signs and symptoms.

$^{124}\text{I}$ -omburtamab distribution showed high deposition and reasonably long retention at the lesion site, enabling delivery of high radiation doses to the lesion with high therapeutic ratios, with low systemic distribution and no observable systemic toxicities. Visually, no cardiac or vascular blood-pool activity was noted, which is important in terms of limiting radiation dose to the blood and marrow. Low blood- and marrow-absorbed dose estimates were thus noted, consistent with the lack of any high-grade hematologic toxicity. This is very important in this population given the concern for possible late effects from radiation in these radiosensitive young patients. Systemic clearance of activity was through renal excretion, visually seen as bladder activity and resulting in the highest (but still low) absorbed dose to the bladder among all distant organs. Visually, systemic activity was otherwise seen in the liver, which subsequently decreased with time (Fig. 5).

There was no distinct difference noted in whole-body or blood kinetics among cohorts related to the increased  $V_d$  of the  $^{124}\text{I}$ -omburtamab. Initial low-volume and low-activity cohorts showed slightly higher blood activities, and the later higher-activity and higher-volume cohorts tended to have somewhat lower blood activities, but these differences were not significant (Fig. 1). For whole-body clearance, there was a trend of increasing retention time from the first cohort to the later cohorts, but again this trend was not significant (Fig. 1). The delivery of higher administered activities required longer infusion times over several hours or longer in cohorts receiving activities of  $120\ \text{MBq}$  or higher. This has evolving implications relating to the logistics of treatment.

Given the localized infusion, high activities were predominantly noted in the lesion and the long residence time allowed for delivery of high absorbed doses to the lesion, with a mean of  $43.2 \pm 33.2\ \text{Gy}$  and ranging as high as  $118.6\ \text{Gy}$  in cohort patients injected with higher activities. There was no significant difference in lesion radiation dose per unit administered activity ( $\text{Gy}/\text{MBq}$ ) among the cohorts.

The long residence time noted with this technique is advantageous, allowing for appropriate monitoring of distribution and dose optimization. Currently, longitudinal monitoring and hence drug scheduling

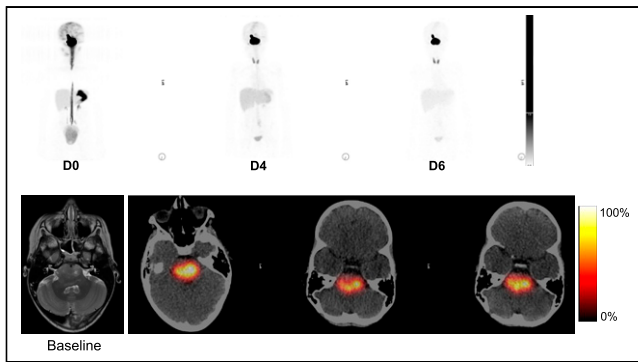


**FIGURE 5.** Example of imaging in 8-y-old patient. Baseline MRI showing  $3.5 \times 2.8$  cm mass centered in pons extending to right cerebral peduncle and brachium pontis.  $^{124}\text{I}$ -omburtamab infusion activity was 148 MBq. Imaging was performed on day of infusion (D0), day 4 (D4), and day 6 (D6), with whole-body and head imaging. High activity is noted at site of tumor until last imaging time point (D6). Infusion time was 10 h. First imaging time point was 16 h after initiation. D1 scan shows activity in spinal canal and systemic activity in liver, stomach, and bladder. Further systemic distribution is noted on D2 as excreted activity in kidneys and bladder, thyroid and stomach, and liver that decreased from D4 to D6.

are not possible with conventional methods of drug distribution monitoring. Surrogate tracers, typically gadolinium contrast agents, as used in functional MRI, are limited in that gadolinium has rapid clearance from the interstitium and is dependent on several factors including concentration, flow, and infusion rate and hence cannot reliably provide an accurate time-dependent measurement of distribution or dose delivery (21,22).

Although  $^{124}\text{I}$ -omburtamab imaging showed high lesion activities and allowed for dose estimation, some limitations are recognized. There are marked variations in lesion activity and radiation dose across patients. Assessment of the lesion uptake and distribution may be influenced by long infusion times. Imaging could only be performed at the end of infusion and in many cases several hours thereafter because of the infusion being completed late at night or in the early morning. In most patients, initial imaging was at least 6–8 h after injection, and in later cohorts, imaging was conducted 24 h or more after the initiation of the infusion. This could have led to some significant internal distribution and clearance from the infusion site. Using the exponential functions fitted to the lesion time–activity data, the activity at the start of the infusions could be estimated, but the resulting estimates may be compromised by the long infusion times and distribution and clearance of the activity over the course of the infusion. The variation in distribution of the administered activity was noted, with some patients showing early clearance via activity tracking down the spinal canal and cerebrospinal fluid flow pathway. The activity and dose equivalents to cerebrospinal fluid and the spinal cord were nonetheless low, with a mean of  $0.41 \pm 0.39$  mSv/MBq (range, 0.01–1.68 mSv/MBq). This distribution was likely related to the flow along the intracerebral path of the canula after removal after infusion, especially in areas proximal to cerebrospinal fluid flow such as the fourth ventricle.

One of the objectives of the initial assessment with activity escalation was to assess the optimal volume of infusate that would allow for complete coverage of the tumor volume. Because the activity concentration in the infusate was constant across all administered activity levels (nominally 37 MBq/mL), the administered activity serves as a surrogate metric of the  $V_i$ . The  $V_i$  increased as the administered activity and therefore volume of administered

activity increased. There was a highly significant linear correlation of the  $V_d$  of activity in the lesion with the administered activity and therefore the  $V_i$ . This linear relationship between  $V_d$  and  $V_i$  has been described using CED in the brain in other settings (16,23). In principle, this may allow for optimization of the treatment delivery, in which a suitable volume matched to the tumor volume may be administered. In the brain stem, mean  $V_d/V_i$  ratios between 2 and 3 are noted (22,24,25). Previously, in an initial analysis, we reported linear dependency of estimated  $V_d$  on  $V_i$  within individual patients across serial time points as well as across patients with a mean  $V_d/V_i$  ratio of  $3.4 (\pm 1.2)$  (16). The data in this larger cohort are similar with a mean  $V_d/V_i$  ratio of  $3.4 (\pm 0.9)$ .

The study shows the feasibility of  $^{124}\text{I}$ -omburtamab for therapeutics of DIPG using intratumoral administration by CED infusion. Further analysis of  $V_d$  and voxel-based dosimetry is under way to better understand the 3-dimensional distribution of dose within the lesion and its impact on response.

## CONCLUSION

Intratumoral CED of  $^{124}\text{I}$ -omburtamab is a theranostic technique that allows for delivery of therapeutic radiation doses to brain lesions. Imaging with  $^{124}\text{I}$ -omburtamab allowed for assessment of lesion radiation doses with escalating administered activities. As a first-ever assessment, to our knowledge, this study shows feasibility of using  $^{124}\text{I}$  as a truly simultaneous imaging and therapeutic isotope.

## DISCLOSURE

Kim Kramer has received support from NIH grants K08 CA072868, R21 CA089935, and R21 CA117076, as well as grant support from Luke's Lollies and Catie Hoch Foundation, the Dana Foundation, the Cure Starts Now, Solving Kids' Cancer, the Lyla Nsouli Foundation, Cookies for Kids' Cancer, the Cristian Rivera Foundation, Battle for a Cure, Cole Foundation, Meryl & Charles Witmer Charitable Foundation, and Tuesdays with Mitch Charitable Foundation. Mark Souweidane has received support from Cristian Rivera Foundation, McKenna Claire Foundation, The Lyonhearted Foundation, Christian Koehler Foundation, Brooke Healey Foundation, Fly a Kite Foundation, Children's Brain Tumor Family Foundation, Joshua's Wish, Lily LaRue Foundation, and Alex's Lemonade Stand Foundation. Memorial Sloan Kettering Cancer Center's (MSK) Radiochemistry and Molecular Imaging Probe Core is funded in part through the NIH/NCI Cancer Center Support Grant P30 CA008748. MSK Center has institutional financial interests related to this research in the form of intellectual property rights and equity interests in Y-mAbs, the company licensing the intellectual property from MSK. Y-mAbs has provided support for this study. Neeta Pandit-Taskar has served as a consultant or advisory board member for or received honoraria from Actinium Pharma, Progenics, Medimmune/AstraZeneca, Illumina, and ImaginAb and conducts research institutionally supported by Y-mAbs, ImaginAb, BMS, Bayer, Clarity Pharma, Janssen, and Regeneron. Pat Zanzonico, Serge Lyashchenko, and Kim Kramer serve as a consultant for Y-mAbs. Ira Dunkel has received consulting fees from AstraZeneca, Day One, GSK, and Pyramid and has served on an advisory board for AstraZeneca and on a data safety and monitoring board for Bristol-Meyers Squibb. He has also been the site PI for clinical trials for Bristol-Meyers Squibb, Genentech, and Novartis (sponsors provided funding to MSK). He served as the Chair of the Pediatric Brain Tumor Consortium (payment made to MSK). No other potential conflict of interest relevant to this article was reported.

## KEY POINTS

**QUESTION:** Is imaging important in optimizing local delivery of therapeutic agent?

**PERTINENT FINDINGS:** This study highlights the role of imaging in the assessment and guidance of novel CED intratumoral delivery of radiolabeled antibodies for therapy. To our knowledge, this is the first-ever use and feasibility proof of  $^{124}\text{I}$  as a simultaneous imaging and therapeutic radionuclide. Delivery of the radiolabeled antibody via CED is feasible, and imaging allows for assessing distribution and dosimetry.  $^{124}\text{I}$  can be used to deliver therapeutic radiation to tumors.

**IMPLICATIONS FOR PATIENT CARE:** Intratumoral CED of  $^{124}\text{I}$ -omburtamab is a theranostic technique that allows for delivery of therapeutic radiation doses for treatment of brain lesions.

## REFERENCES

1. Dunkel IJ, Garvin JH Jr, Goldman S, et al. High dose chemotherapy with autologous bone marrow rescue for children with diffuse pontine brain stem tumors. Children's Cancer Group. *J Neurooncol.* 1998;37:67–73.
2. Kaplan AM, Albright AL, Zimmerman RA, et al. Brainstem gliomas in children: a Children's Cancer Group review of 119 cases. *Pediatr Neurosurg.* 1996;24:185–192.
3. Frazier JL, Lee J, Thomale UW, Noggle JC, Cohen KJ, Jallo GI. Treatment of diffuse intrinsic brainstem gliomas: failed approaches and future strategies. *J Neurosurg Pediatr.* 2009;3:259–269.
4. Korones DN, Fisher PG, Kretschmar C, et al. Treatment of children with diffuse intrinsic brain stem glioma with radiotherapy, vincristine and oral VP-16: a Children's Oncology Group phase II study. *Pediatr Blood Cancer.* 2008;50:227–230.
5. Pandit-Taskar N, Zanzonico PB, Kramer K, et al. Biodistribution and dosimetry of intraventricularly administered  $^{124}\text{I}$ -omburtamab in patients with metastatic leptomeningeal tumors. *J Nucl Med.* 2019;60:1794–1801.
6. Kramer K, Smith-Jones P, Humm J, et al. Radioimmunotherapy (RIT) of central nervous system (CNS) and leptomeningeal (LM) cancers: phase I study of intracranial I-131-8H9 [abstract]. *Neuro-oncol.* 2008;10:513.
7. Sandberg DI, Edgar MA, Souweidane MM. Convection-enhanced delivery into the rat brainstem. *J Neurosurg.* 2002;96:885–891.
8. Souweidane MM. Editorial: convection-enhanced delivery for diffuse intrinsic pontine glioma. *J Neurosurg Pediatr.* 2014;13:273–274.
9. Szycho E, Walker D, Collins P, et al. Clinical experience of convection-enhanced delivery (CED) of carboplatin and sodium valproate into the pons for the treatment of diffuse intrinsic pontine glioma (DIPG) in children and young adults after radiotherapy. *Int J Clin Oncol.* 2021;26:647–658.
10. van Vuurden DG. Convection-enhanced delivery: chemosurgery in diffuse intrinsic pontine glioma. *Lancet Oncol.* 2018;19:1001–1003.
11. Barua NU, Lowis SP, Woolley M, O'Sullivan S, Harrison R, Gill SS. Robot-guided convection-enhanced delivery of carboplatin for advanced brainstem glioma. *Acta Neurochir (Wien).* 2013;155:1459–1465.
12. Heiss JD, Jamshidi A, Shah S, et al. Phase I trial of convection-enhanced delivery of IL13-Pseudomonas toxin in children with diffuse intrinsic pontine glioma. *J Neurosurg Pediatr.* 2018;23:333–342.
13. Modak S, Kramer K, Gultekin SH, Guo HF, Cheung NK. Monoclonal antibody 8H9 targets a novel cell surface antigen expressed by a wide spectrum of human solid tumors. *Cancer Res.* 2001;61:4048–4054.
14. Xu H, Cheung IY, Guo HF, Cheung NK. MicroRNA miR-29 modulates expression of immunoinhibitory molecule B7-H3: potential implications for immune based therapy of human solid tumors. *Cancer Res.* 2009;69:6275–6281.
15. Luther N, Zhou Z, Zanzonico P, et al. The potential of theragnostic  $^{124}\text{I}$ -8H9 convection-enhanced delivery in diffuse intrinsic pontine glioma. *Neuro-oncol.* 2014;16:800–806.
16. Souweidane MM, Kramer K, Pandit-Taskar N, et al. Convection-enhanced delivery for diffuse intrinsic pontine glioma: a single-centre, dose-escalation, phase I trial. *Lancet Oncol.* 2018;19:1040–1050.
17. Fanchon LM, Beattie BJ, Pentlow K, Larson SM, Humm JL. Optimizing reconstruction parameters for quantitative  $^{124}\text{I}$ -PET in the presence of therapeutic doses of  $^{131}\text{I}$ . *EJNMMI Phys.* 2021;8:50.
18. Barrett PH, Bell BM, Cobelli C, et al. SAAM II: simulation, analysis, and modeling software for tracer and pharmacokinetic studies. *Metabolism.* 1998;47:484–492.
19. Weber DA, Eckerman KF, Dillman LT, Ryman JC. *MIRD: Radionuclide Data and Decay Schemes.* Society of Nuclear Medicine; 1975:218–219.
20. Eckerman KF, Endo A. *MIRD: Radionuclide Data and Decay Schemes.* 2nd ed. Society of Nuclear Medicine; 1989:305–307.
21. Tosi U, Souweidane M. Convection enhanced delivery for diffuse intrinsic pontine glioma: review of a single institution experience. *Pharmaceutics.* 2020;12:660.
22. Chittiboyna P, Heiss JD, Warren KE, Lonser RR. Magnetic resonance imaging properties of convective delivery in diffuse intrinsic pontine gliomas. *J Neurosurg Pediatr.* 2014;13:276–282.
23. Luther N, Cheung NK, Dunkel IJ, et al. Intraparenchymal and intratumoral interstitial infusion of anti-glioma monoclonal antibody 8H9. *Neurosurgery.* 2008;63:1166–1174, discussion 1174.
24. Lonser RR, Warren KE, Butman JA, et al. Real-time image-guided direct convective perfusion of intrinsic brainstem lesions. *J Neurosurg.* 2007;107:190–197.
25. Voges J, Reszka R, Gossmann A, et al. Imaging-guided convection-enhanced delivery and gene therapy of glioblastoma. *Ann Neurol.* 2003;54:479–487.